# LiTFSI Structure and Transport in Ethylene Carbonate from Molecular Dynamics Simulations

**Oleg Borodin*,† and Grant D. Smith†,‡**

*Department of Materials Science & Engineering, Room 304, 122 South Central Campus Drive, University of Utah, Salt Lake City, Utah 84112-0560, and Department of Chemical Engineering, University of Utah, Salt Lake City, Utah 84112*

*Received: October 30, 2005; In Final Form: January 10, 2006*

Molecular dynamics (MD) simulations using a many-body polarizable force field were performed on ethylene carbonate (EC) doped with lithium bistrifluoromethanesulfonamide (LiTFSI) salt as a function of temperature and salt concentration. At 313 K $Li^+$ was coordinated by 2.7−3.2 EC carbonyl oxygen atoms and 0.67−1.05 $TFSI^-$ oxygen atoms at EC:Li = 10 and 20 salt concentrations. In completely dissociated electrolytes, however, $Li^+$ was solvated by approximately 3.8 carbonyl oxygen atoms from EC on average. The probability of ions to participate ion aggregates decreased exponentially with an increase in the size of the aggregate. Ion and solvent self-diffusion coefficients and conductivity predicted by MD simulations were in good agreement with experiments. Approximately half of the charge was transported by charged ion aggregates with the other half carried by free (uncomplexed by counterion) ions. Investigation of the $Li^+$ transport mechanism revealed that contribution from the $Li^+$ diffusion together with its coordination shell to the total $Li^+$ transport is similar to the contribution arising from $Li^+$ exchanging solvent molecules in its first coordination shell with solvents from the outer shells.

## I. Introduction

Secondary (rechargeable) lithium batteries with liquid electrolytes are widely used in portable electronics and are being extensively investigated for use in environmentally friendly and efficient electric vehicles and hybrid-electric vehicles. Ethylene carbonate (EC) is one of the most commonly used solvents for mixed solvent electrolytes aimed at lithium battery applications. It has high melting point of 36.4 °C, high dielectric constant (≈90) and an acceptable viscosity (1.9 cP at 40 °C). High dielectric constant promotes ion dissociation, which is important because neutral salt aggregates and ion pairs do not carry charge and, therefore, do not contribute to charge transport, while a relatively low viscosity fosters ion diffusion as ion diffusion in liquid electrolytes have been found to be inversely proportional to solvent viscosity.[1] Further lowering of the electrolyte melting point, a decrease in electrolyte viscosity, and improved low temperature performance are achieved by mixing EC with other low viscosity solvents such as dimethyl carbonate. Importantly, EC reduction products are known to form an effective solid electrolyte interphase layer on graphitic anodes that help prevent electrolyte decomposition and provide good reversibility for lithium intercalation/deintercalation. However, despite widespread use of EC in lithium batteries and a number of experimental and simulation studies of EC/$Li^+$ interactions,[2−4] the mechanism of ion transport and the nature and size of ion aggregates in EC electrolytes are still largely unknown.

Molecular dynamics (MD) simulations are well suited for exploring structure and transport mechanisms in liquid electrolytes relevant to secondary lithium batteries since ions move sufficiently far on times scales accessible to MD simulations (multiple nanoseconds) to allow determination of transport properties. The lifetime of ion aggregates and solvation structure is also sufficiently short to allow equilibrium sampling on the MD time scale. However, to provide useful and reliable insight into structure and transport in these materials, the force fields employed in the simulations must capture accurately all essential physics embodied in the interactions between ions and solvent. While results from several MD simulation studies of EC,[2−4] propylene carbonate (PC)[5] and $\gamma$-butyrolactone (GBL)[6] have been reported, most of them have considered only a single $Li^+$ cation and have concentrated on understanding the first $Li^+$ solvation shell. Validation of the force fields used in these simulations[2,4,6] was limited to comparing the $Li^+$ self-diffusion coefficient at infinite dilution with extrapolated experimental data. Electrolyte conductivity over wide concentration range of salt concentration was reported only in one simulation study of PC/$LiBF_4$.[5] Unfortunately, these simulations yielded a maximum conductivity of a factor of 6 lower than the experimental value revealing serious shortcomings of the simulations likely due to the force field employed.

In this work we report on MD simulations of EC doped with lithium bistrifluoromethanesulfonamide ($LiCF_3SO_2NSO_2CF_3$ denoted at LiTFSI). $TFSI^-$ anion was chosen because it is a large anion with delocalized charge and it usually has lower binding to $Li^+$ and yield more free (uncomplexed by anion) $Li^+$ cations available for charge transport compared to conventional anions such as $BF_4^-$, $PF_6^-$. We utilize a recently developed accurate quantum chemistry-based many-body polarizable force field[7] in order to provide a detailed picture of ion aggregation and elucidate the $Li^+$ transport mechanisms in EC/LiTFSI.

## II. Molecular Dynamics Simulations Methodology

A version of the molecular dynamics simulation package *Lucretius*[8] that includes many-body polarization was used for

† Department of Materials Science & Engineering, University of Utah.
‡ Department of Chemical Engineering, University of Utah.

10.1021/jp056249q CCC: $33.50 
Published on Web 02/15/2006

**TABLE 1: Composition of the $Li^+$ First Solvation Shell**

| temp (K) | no. of EC in a simulation cell, $N_{EC}$ | salt concn (EO:Li) | length of sampling runs (ns) | no. of oxygen atoms within 2.8 Å of a $Li^+$ | | | |
|---|---|---|---|---|---|---|---|
| | | | | Oc | O($TFSI^-$) | Oc+O($TFSI^-$) | Oe |
| 313 | 400 | 20 | 4.0 | 3.00 | 0.75 | 3.75 | 0.50 |
| 313 | 200 | 20 | 5.9 | 3.17 | 0.67 | 3.84 | 0.43 |
| 313 | 400 | 10 | 3.2 | 2.68 | 1.05 | 3.73 | 0.50 |
| 313 | 200 | 10 | 20 | 2.8 | 0.94 | 3.74 | 0.48 |
| 333 | 200 | 10 | 20 | 2.69 | 1.05 | 3.74 | 0.48 |
| 363 | 200 | 10 | 3 | 2.78 | 0.92 | 3.7 | 0.52 |
| 363 | 200 | 10[a] | 1.5 | 3.83 | 0 | 3.83 | 0.36 |

[a] Dissociated.

all MD simulations. A three-dimensional, periodic cubic simulation cell consisted of 200 or 400 EC molecules and 10 or 20 LiTFSI molecules corresponding to EC:Li ratios of 20 and 10 was utilized. Simulated electrolytes with 200 EC molecules per simulation cell are denoted as small systems, while electrolytes with 400 EC molecules per cell are denoted as large systems. Simulation results for small and large systems will be compared to ensure that reported results are independent of the size of the simulation cell. All electrolytes were created in the gas phase corresponding to a cell (linear) dimension of approximately 80−90 Å. The cell size was reduced to yield densities corresponding to an average pressure of 1 atm at each temperature simulated (313, 333, 363, and 393 K for EC:Li = 10:1 and 313 K for EC:Li = 20:1). Following equilibration runs of 2−4 ns performed in the *NPT* ensemble at 1 atm the long sampling runs were performed in the *NVT* ensemble with the run lengths listed in Table 1. The equilibrated simulation cells had linear dimensions ≈29−38 Å depending on temperature and composition.

A Nose−Hoover thermostat and a barostat[9] were used to control the temperature and pressure, while bond lengths were constrained using the Shake algorithm.[10] The Ewald summation method was used for treatment of long-range electrostatic forces between partial charges and between partial charges and induced dipoles for the many-body polarizable potential. A tapering function was used for scaling the induced dipole−induced dipole interactions to zero at the cutoff of 10 Å, with scaling starting at 9 Å. A multiple time step reversible reference system propagator algorithm was employed,[11] with a time step of 0.5 fs for bonding, bending, and torsional motions, a 1.5 fs time step for nonbonded interactions within a 6.5 Å sphere and a 3.0 fs time step for nonbonded interactions between 6.5 and 10.0 Å, and the reciprocal space part of the Ewald summation.

Two additional simulations with force fields modified as described below were performed at for the EC:Li = 10 electrolyte with 200 EC molecules in a box at 363 K for 1.5−2 ns after 1 ns equilibration. In the first simulation, the repulsion between $Li^+$/$TFSI^-$ was increased in order to obtain complete salt dissociation. In the second simulation, the $Li^+$/EC short range attraction was increased in order to significantly increase the residence times of EC molecules in the first solvation shell of $Li^+$.

## III. Structural Properties

We begin examination of the structure of the $Li^+$ solvation shell with analysis of the $Li^+$−O radial distribution functions (RDF) shown in Figure 1. $Li^+$ is strongly coordinated by carbonyl oxygen atoms (Oc) from EC and oxygen atoms from $TFSI^-$ anions. The position of the first peak of the Li−Oc RDF shown in Figure 1a is at ≈1.95 Å for all concentrations and temperatures investigated. Even the electrolyte with the decreased $Li^+$/$TFSI^-$ interactions that resulted in complete ion

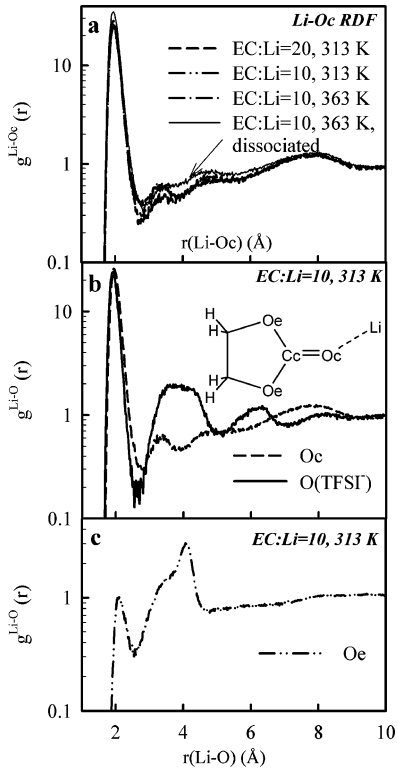


**Figure 1.** Radial distribution functions $g^{Li-O}(r)$ for EC/LiTFSI with 200 EC molecules from MD simulations. Results for EC/LiTFSI simulations using large simulation cell ($N_{EC}$ = 400) are similar and, therefore, not shown.

dissociation has the same position of the Li−Oc RDF, which is, interestingly, similar to the Li−Oc separation of 1.95 Å found in a quantum chemistry study of the $Li^+(EC)_4$ gas-phase cluster.[4] Previous simulations of EC/$Li^+$ and EC/$LiClO_4$,[2,3] however, reported systematically shorter Li−Oc separations resulting in positions of the first peak of Li−Oc RDF at 1.7−1.8 Å, that is 0.15−0.25 Å closer than found in this work. The magnitude of the first Li−Oc peak is around 25−35, which is about a factor of 2 smaller than the values observed in previous simulations,[2−4] thus indicating a significantly less pronounced structuring of the $Li^+$/EC observed in our work compared to previous simulations.[2,3]

The position and magnitude of the first peak of the Li/O($TFSI^-$) RDF almost coincides with those for the Li−Oc RDF, indicating that the free energies of $Li^+$ binding to Oc of EC and O($TFSI^-$) are comparable in electrolyte solutions. On the other hand, $Li^+$ has a much smaller tendency to be solvated by ether oxygen (Oe) atoms of EC (see Figure 1) compared to other oxygen atom types (Oc and O($TFSI^-$)) as seen from the Li−Oe RDF that shows only a small peak at 2.1 Å. A much more pronounced peak of the Li−Oe RDF at 4.05 Å (note the log

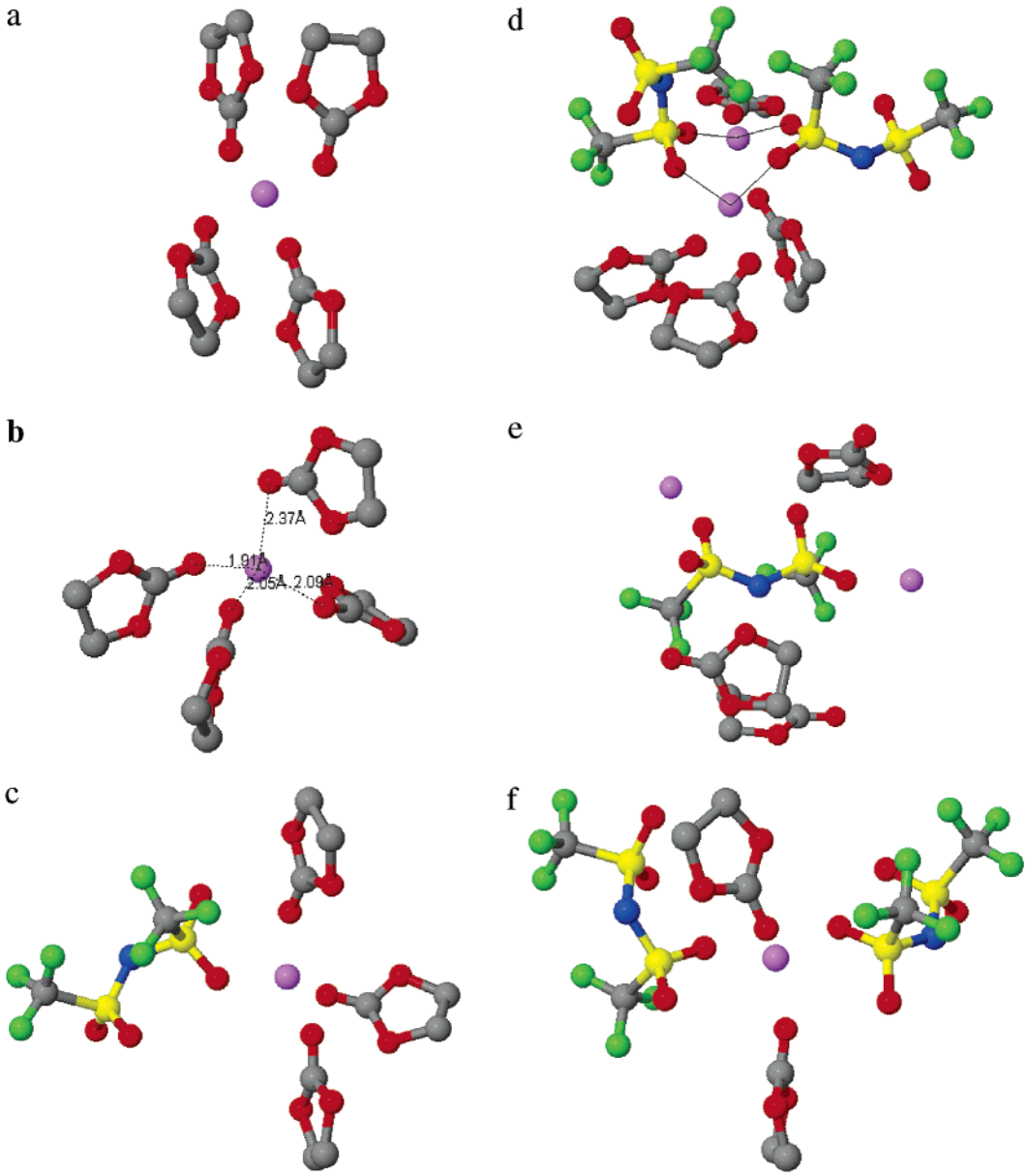


**Figure 2.** Representative snapshots from MD simulations illustrating various compositions of the $Li^+$ first solvation shell. Hydrogen atoms are not shown for clarity.

scale for $g^{Li-O}(r)$ in Figure 1c) corresponds to EC coordinated toward $Li^+$ as shown in a schematic picture in Figure 1b and Figure 2a.

The average composition of the $Li^+$ first solvation shell is summarized in Table 1 for EC:Li = 10 and 20 salt concentrations for small and large simulations cell containing 200 and 400 EC molecules. $Li^+$ is solvated primarily by carbonyl oxygens (Oc) with some contributions from Oe and O($TFSI^-$). The $Li^+$ coordination by Oc and O($TFSI^-$) in a small simulation box ($N_{EC}$ = 200) is similar to its coordination in a large simulation box containing 400 EC molecules ($N_{EC}$ = 400) as seen from Table 1, thus indicating that the predicted structure of the $Li^+$ coordination is only weakly dependent on the simulation cell with the larger simulation cell leading to each $Li^+$ having 0.1 O($TFSI^-$) more in its first coordination shell compared to $Li^+$ coordination in a smaller simulation cell.

At EO:Li = 20, each $Li^+$ is coordinated by ≈3.0−3.2 carbonyl oxygen atoms from EC, while in a dissociated electrolyte $Li^+$ has 3.8 carbonyl oxygen atoms from EC in its first solvation shell and often forms structures similar to those shown in Figure 2a,b. The number of EC molecules coordinating around a $Li^+$ is somewhat less than was found from analysis of Raman spectroscopic studies[12] of EC/$LiClO_4$ for salt concentrations from 0.1 to 1 M and conclusions from previous simulations[2−4] that indicated four EC present in the $Li^+$ first solvation shell. However, electrospray ionization mass spectroscopy measurements[13] of gas-phase $Li^+EC_n$ clusters found evidence of only $Li^+EC_2$ and $Li^+EC_3$ clusters and no $Li^+EC_4$ clusters. Quantum chemistry studies by Wang et al.[14] showed that addition of the fourth EC to the $Li^+EC_3$ cluster is favorable only by 2.4 kcal/mol, pointing to the possibility that the $Li^+$-$EC_4$ cluster is not very stable in a gas phase, consistent with the electrospray ionization mass spectroscopy measurements.[13] We believe that our predictions from our MD simulations of a complete $Li^+$ coordination shell consisting of 3.8 EC molecules on average for the completely dissociated electrolyte mimicking dilute solution conditions are consistent with the results of the above-mentioned quantum chemistry and electrospray ionization mass spectroscopy measurements. For example, if we consider only very tightly bound EC to a $Li^+$ ($r_{Li-Oc}$ < 2.1 Å), we obtain

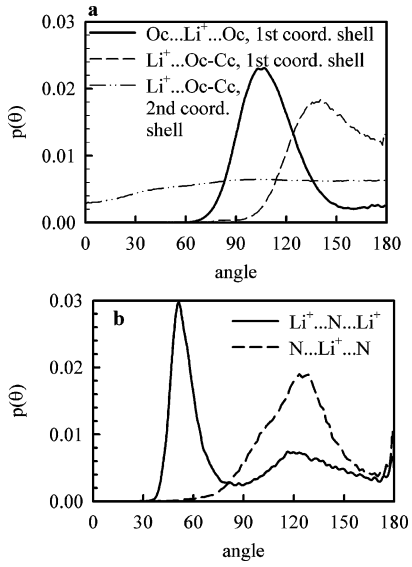


**Figure 3.** Distribution of angles for molecules in the $Li^+$ first coordination shell for EC:Li = 10 at 313 K, $N_{EC} = 200$.

data showing that $Li^+$ is coordinated by three EC carbonyl oxygens. The $Li^+$ coordination shown in Figure 2b is an example of a $Li^+$ having 4 EC in its complete coordination shell ($r_{Li-Oc}$<2.8 Å), out of which only 3 EC are tightly bound ($r_{Li-Oc}$<2.1 Å). We admit that the definition for tightly bound EC is somewhat arbitrary but it allows us to reconcile results of Raman spectroscopic studies possibly yielding complete $Li^+$ coordination and electrospray ionization mass spectroscopy measurements that sense only tightly bound $Li^+$/EC coordinations. Finally, we note that doubling salt concentration (from EC:Li = 20 to 10) increases the number of O($TFSI^-$) in the $Li^+$ first solvation shell while the total number of oxygen atoms in the solvation shell is approximately independent of salt concentration, as shown in Table 1.

More details about arrangement of EC molecules in the $Li^+$ first solvation shell is obtained from analysis the Oc···$Li^+$···Oc and $Li^+$···Oc−Cc angle probability p($\theta$) calculated according to the following

$$p(\theta) = \frac{N_\theta}{\sin(\theta)\sum N_\theta} \qquad (1)$$

where $N_\theta$ is the number of the Oc···$Li^+$···Oc and $Li^+$···Oc−Cc angles with the angle $\theta$ and the probability function is normalized by sin($\theta$). The Oc···$Li^+$···Oc angle probability is shown in Figure 3a. It exhibits a well pronounced peak around 105° indicating that carbonyl oxygen atoms form a tetrahedral like arrangement around $Li^+$ such as shown in Figure 2. The Cc−Oc bond of EC is usually tilted from the Oc···$Li^+$ direction (see scheme in Figure 1b) with the most probable $Li^+$···Oc−Cc angle of around 140° as shown in Figure 3a, which is remarkably similar to the value of 142° found in a gas-phase quantum chemistry study[4] of the $Li^+(EC)_4$ cluster level but is lower than values of 160−170° reported in previous MD simulations.[2,4] Interestingly, EC molecules in the $Li^+$ second solvation shell showed very little orientational correlation between the $Li^+$···Oc direction and direction of the Oc−Cc bond indicating that the EC molecules in the $Li^+$ first solvation shell effectively screens most of the $Li^+$/EC interactions beyond its first solvation shell.

At the next step we characterize the $Li^+$ coordination by $TFSI^-$ anions. We found that each $TFSI^-$ anion in the coordination shell of a $Li^+$ contributes only one oxygen out of four possible to $Li^+$ coordination with the other three oxygen atoms of $TFSI^-$ anions being outside of the $Li^+$ first solvation shell (Figure 2c−e); thus, the number of O($TFSI^-$) atoms in the $Li^+$ first solvation shell is equivalent to the number of $TFSI^-$ anions forming anion−cation contacts.

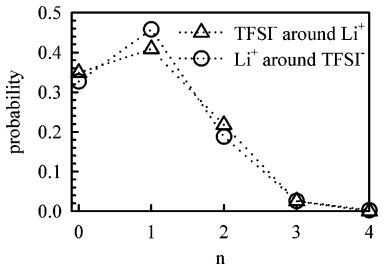


**Figure 4.** Probability of finding $n$ of $Li^+$ within 5 Å of N($TFSI^-$) and N($TFSI^-$) with 5 Å of $Li^+$. Separation of 5 Å corresponds to the position of the well after the first peak of $Li^+$···N($TFSI^-$) RDF.

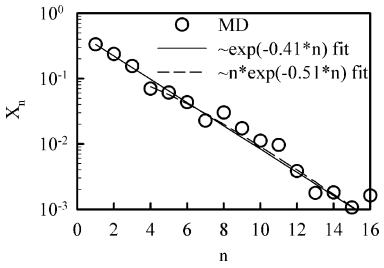


**Figure 5.** Ion cluster size ($n$) distribution for EC:Li = 10 at 313 K, $N_{EC} = 200$.

The number of $Li^+$ ions in the first solvation shell of $TFSI^-$ and the number of $TFSI^-$ ions in the first solvation shell of $Li^+$ are shown in Figure 4 for EC:Li = 10 at 313 K and are qualitatively similar to the data at other temperatures and concentrations. Concentrations of free (without a counterion in the first solvation shell, i.e., $n = 0$) $Li^+$ cations and $TFSI^-$ anions are approximately equal to each other. Figure 4 indicates that the highest probability is to find only one counterion in both $Li^+$ and $TFSI^-$ solvation shells. However, a significant (≈20%) probability exists for finding two counterions in the ion solvation shell. Analysis of the counterions arrangement in the solvation shell indicated three most probable scenarios schematically shown in Figure 2c−e and confirmed via analysis of the N($TFSI^-$)···$Li^+$···N($TFSI^-$) and $Li^+$···N($TFSI^-$)···$Li^+$ angle probabilities shown in Figure 3b. The $Li^+$···N(TFSI−)···$Li^+$ angle distribution is bimodal with peaks at ≈52° and ≈120°. The somewhat surprising peak at 52° corresponds to structures shown in Figure 2d in which two lithiums are connecting two $TFSI^-$ anions. The cation−anion binding energy in such structured is facilitated by polarizing $TFSI^-$ anions by two lithiums located on the same side of each $TFSI^-$ anion. Similar clusters involving two lithiums coordinating two dialkyl dicarbonates were found energetically favorable in a recent quantum chemistry study.[15] The other peak of the $Li^+$···N($TFSI^-$)···$Li^+$ angle distribution function corresponds to the structure shown in Figure 2e. The N($TFSI^-$)···$Li^+$···N($TFSI^-$) RDF has a well pronounced peak at 128° corresponding to the structure shown in Figure 2f, in which a $Li^+$ cation is bridging two $TFSI^-$ anions.

Ions coordinated by counterions connect with each other and form ion aggregates. The probability of finding an ion being a part of an ion aggregate containing $n$-ions ($X_n$) is shown in Figure 5. This distribution shows a monotonic decay and is well described by an exponential function of ~exp(−$Cn$), where C

**TABLE 2: Ion Self-Diffusion Coefficients (D), Conductivity ($\lambda$), and Extent of Ion Uncorrelated Motion ($\alpha$) from MD Simulations with Large ($N_{EC} = 400$) and Small ($N_{EC} = 200$) Simulations Cells and Experiments[1] for EC:Li = 20 at 313 K**

| | $D$ ($10^{-10}$ m$^2$/s) | | | | |
|---|---|---|---|---|---|
| | EC | $TFSI^-$ | $Li^+$ | $\lambda$ (mS/cm) | $\alpha$ |
| MD ($N_{EC} = 400$) | 5.8 | 2.9 | 2.9 | 9.9 | 0.72 |
| MD ($N_{EC} = 200$) | 5.3 | 2.8 | 2.8 | 10.8 | 0.82 |
| experiments[1] | 4.3 | 3.1 | 2.1 | 8.3 | 0.67 |

is constant. Simple theoretical considerations for one-dimensional aggregates with no preferred cluster size[16] predict distribution scaling as $\sim n \exp(-Cn)$ that also fits distribution calculated from MD simulations for $n > 3$.

## IV. Transport Properties

The self-diffusion coefficient $D$ was calculated using the Einstein relation

$$D = \lim_{t\to\infty} \frac{\langle \mathrm{MSD}(t) \rangle}{6t} \tag{2}$$

where MSD($t$) is mean-square displacement of a molecule center of mass during time $t$ and $\langle\ \rangle$ denotes an ensemble average. Ion and solvent self-diffusion coefficients have been measured in pgf-NMR experiments[1] for EC:Li = 20 at 313 K and are summarized in Table 2 together with EC and ion with self-diffusion coefficients predicted from MD simulations for large and small simulation cells. Size of the simulation cell does not significantly influence ion and solvent self-diffusion coefficients but leads to a slightly more correlated ion motion for the larger simulation cell as reflected by a smaller extent of ion uncorrelated motion ($\alpha$) for $N_{EC} = 400$. This is consistent with a slightly higher number of $TFSI^-$ coordinating $Li^+$ in a larger simulation cell as shown in Table 1. The $TFSI^-$ self-diffusion coefficient was predicted by simulations the most accurately, while the self-diffusion coefficients of EC and $Li^+$ from MD simulations were approximately 30% higher than those from experiments. We think the agreement between simulation predictions and experiments is good especially taking into account that no force field parameters were adjusted to achieve this agreement.

Ionic conductivity from MD simulations is calculated using the Einstein relation

$$\lambda = \lim_{t\to\infty} \frac{e^2}{6tVk_BT} \sum_{ij}^{N} z_i z_j \langle [\mathbf{R}_i(t) - \mathbf{R}_i(0)][\mathbf{R}_j(t) - \mathbf{R}_j(0)] \rangle \tag{3}$$

where $e$ is the electron charge, $V$ is the volume of the simulation box, $k_B$ is Boltzmann's constant, $T$ is the temperature, $t$ is time, $z_i$ and $z_j$ are the charges over ions $i$ and $j$ in electrons, $\mathbf{R}_i(t)$ is the displacement of ion $i$ during time $t$, the summation is performed over all ions, $\langle\ \rangle$ denotes the ensemble average, and $N$ is the total number of ions in the simulation box. The diagonal terms in eq 3 ($i = j$) yield the contribution to ionic contribution from ion self-diffusion. Off-diagonal terms arising from cations and anions moving in the same direction (correlated ion motion) decrease the total charge transport. The degree of uncorrelated ion motion ($\alpha$) is typically measured as ratio of the collective (total) charge transport to the charge transport due to self-diffusion only (a limit of completely dissociated and uncorrelated motion) and is given by

$$\lambda = \alpha Ne^2(D_+ + D_-)/Vk_BT \tag{4}$$

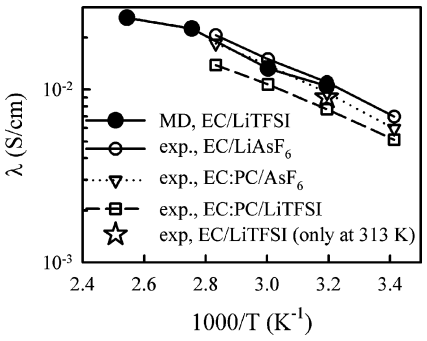


**Figure 6.** Conductivity of MD simulations for EC:Li = 10 (1.1−1.2 M) and from experiments[17,18] at 1 M salt concentration.

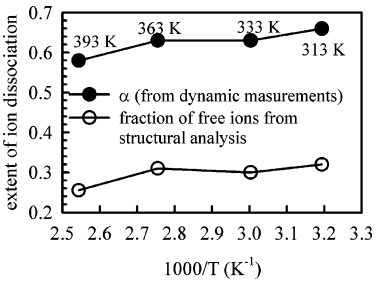


**Figure 7.** Fraction of free ions and the extent of ion uncorrelated motion ($\alpha$) for EC:Li = 10.

Ion conductivity and degree of uncorrelated of ion motion ($\alpha$) from a combination of the pgf-NMR and conductivity measurements[1] and MD simulations are compared in Table 2. Conductivity from MD simulations is up to 30% higher than the experimental value, which we consider to be good agreement. Importantly, MD simulations provide a good prediction of the degree of uncorrelated of ion motion ($\alpha$), indicating that the state of ion aggregation is adequately predicted by the developed force field. We could not find experimental data on temperature dependence of EC/LiTFSI conductivity; therefore, we compared MD simulation predictions with measured conductivities on similar electrolytes (EC/$LiAsF_6$, EC:PC/LiTFSI)[17] as a function of temperature and conductivity of EC/LiTFSI reported only at 313 K[18] in Figure 6 which showed good agreement between MD predictions and experiments.

The temperature dependence of the degree of uncorrelated ($\alpha$) of ion motion is shown in Figure 7 together with the fraction of free ions obtained from structural analysis. Both the fraction of free ions and $\alpha$ show a slight decrease with increasing temperature indicating a slightly increased ion clustering with increasing temperature. Interestingly, the magnitude of $\alpha$ is much larger than the fraction of free ions. This is possible only if charged ion aggregates contribute to charge transport. We attempted to quantify diffusion of each type of charged species. At 313 K, EC:Li = 10 we found that diffusion of free $Li^+$ and $TFSI^-$ was approximately 30% faster than the average ion diffusion, while diffusion of $Li^+$ and $TFSI^-$ that were coordinated by two counterions in their first solvation shell was ≈22% slower than the average ion diffusion. Using cluster distribution from Figure 5 and assuming that clusters with odd $n$ have a charge of one electron and clusters with even size are neutral, we calculated $\alpha$ as

$$\alpha = X_n D_n |z_n| / D(\text{all ions}) \tag{5}$$

where $D_n$ is a diffusion coefficient of the cluster of size $n$ assumed to be equal to $D(Li^+$ complexed by 2 $TFSI^-) \approx D(TFSI^-$ complexed by 2 $Li^+)$ for $n \geq 3$, $z_n$ is a charge of a

**TABLE 3: Properties of the EC/LiTFSI Electrolytes with EC:Li = 10 at 363 K**

| | $\tau_{Li^+/EC}$ (ns) | $D^{EC}$ ($10^{-10}$ m$^2$/s) | $D^{TFSI^-}$ ($10^{-10}$ m$^2$/s) | $D^{Li^+}$ ($10^{-10}$ m$^2$/s) |
|---|---|---|---|---|
| original force field | 0.094 | 9.4 | 4.9 | 5.1 |
| dissociated electrolyte: decreased $Li^+$/$TFSI^-$ interactions | 0.11 | 8.4 | 4.7 | 5.6 |
| dissociated electrolyte with reduced EC exchange in the $Li^+$ solvation shell: decreased $Li^+$/$TFSI^-$ and increased $Li^+$/EC interactions | 1.16 | 6.0 | 3.7 | 2.5 |

cluster of size $n$, and $X_n$ is the probability of an ion to be in a cluster of size $n$. Using eq 5, we obtain $\alpha$ of 0.3 if the charge is carried only by free $Li^+$ and free $TFSI^-$, and $\alpha$ of 0.57 when diffusion of all charged species was included, which is similar to 0.67 obtained from eq 4 for $\alpha$. An important conclusion from the above analysis is that approximately half of the charge at EC:Li = 10 salt concentration is carried by charged aggregates with another half being carried by free ions.

## V. $Li^+$ Transport Mechanism

Having validated the $Li^+$ coordination and ion transport properties for the EC/LiTFSI electrolyte predicted by MD simulations through comparison with experiment, we are now in a position to explore mechanisms of ion transport in detail. Specifically, we want to understand how often EC and $TFSI^-$ molecules from the first $Li^+$ solvation shell exchange with molecules in the second solvation shell and how much this exchange contributes to the $Li^+$ transport. The distributions residence time for the Oc, Oe and O($TFSI^-$) to be present in the $Li^+$ first solvation shell were calculated using eq 6

$$P_{O-Li}(t) = \langle H(t)H(0)\rangle \tag{6}$$

where $H(t)$ is 1 if a given species (Oc,Oe, O($TFSI^-$)) is solvated by a given $Li^+$ and 0 otherwise. To eliminate contribution to $P_{O-Li}(t)$ from molecules that left the solvation shell for a relatively long time and returned afterward, we considered species that were absent from the $Li^+$ first solvation shell for longer than half the mean residence time as new species. This additional modification resulted in residence times for the $Li^+$/Oc and $Li^+$/O($TFSI^-$) of 20−30% shorter than that from calculations without such modification. The residence time was calculated as integral from zero to infinity to the stretched exponential $\exp(-(t/\tau)^\beta)$ fits to the $P_{O-Li}(t)$ distribution functions and are shown in Figure 8. The Oc and O($TFSI^-$) have the longest residence time in the $Li^+$ first solvation shell, whereas Oe atoms leave $Li^+$ first solvation very quickly (within a few ps) indicating that complexes with Li···Oe complexes are short-lived.

Using self-diffusion coefficient data and residence times we estimated that during one $Li^+$/Oc residence time a $Li^+$ moves $\approx$ 4−5 Å, i.e., on the order of the size of one EC molecule, suggesting that a $Li^+$ cation does not diffuse together with its

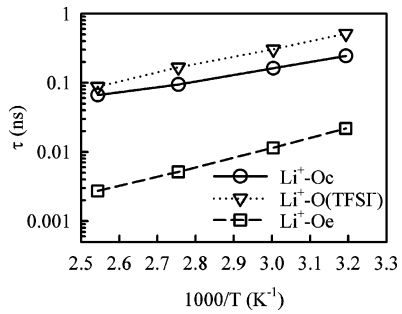


**Figure 8.** Temperature dependence of the Li−O (O = Oc,Oe, O$TFSI^-$) residence times for EC:Li = 10.

first solvation shell for long periods of time. In other words, there is a significant contribution to $Li^+$ transport from the structure-diffusion mechanism in which $Li^+$ moves by exchanging EC molecules instead of moving together with its first solvation shell as sometimes assumed during analysis of experimental data.[1]

MD simulations give us a unique ability to estimate the structure diffusion contribution to the overall $Li^+$ diffusion coefficient by performing simulations in which we essentially do not allow EC exchange in the first $Li^+$ solvation shell during the simulations. This is accomplished by increasing the $Li^+$/EC short range interaction in order to significantly increase the EC residence time in the $Li^+$ first solvation shell. However, increasing the $Li^+$/EC interactions also results in complete dissociation of the $Li^+$/$TFSI^-$ ion pairs and aggregates that potentially might influence ion transport. To understand the influence of $Li^+$/$TFSI^-$ dissociation on ion transport, first we performed additional simulations with the decreased $Li^+$/$TFSI^-$ interactions and other interactions left unchanged.

The $Li^+$/EC residence times, solvent and ion diffusion coefficients for the original and modified force fields are shown in Table 3. Decreasing the $Li^+$/$TFSI^-$ interactions has a minor effect of the $Li^+$/EC residence times and ion diffusion coefficients. The solvent diffusion coefficient decreased by 10% because additional EC became involved in the relatively slow-moving EC−$Li^+$ complexes, while the $Li^+$ self-diffusion increased by 10% as $Li^+$ cations solvated only by EC move faster than the $Li^+$ cations that are part of ion pairs and aggregates as discussed above.

Increasing the $Li^+$/EC interactions does not change the number of EC coordinating each $Li^+$ ($\approx$3.8 EC) but increases the $Li^+$/EC residence time by an order of magnitude demonstrating that EC molecules in the $Li^+$ first solvation shell are essentially moving together with $Li^+$ cations. In this electrolyte $Li^+$ cations that move together with its solvation shell have a self-diffusion coefficient approximately half of that obtained when $Li^+$ cations exchange of EC molecules in the solvation shell via structure-diffusion mechanism. Therefore, we conclude that the structure-diffusion mechanism is responsible for a half of the $Li^+$ diffusion. Table 3 also shows that the EC and $TFSI^-$ diffusion coefficients decreased by 29% and 21%, respectively, when exchange of EC molecules in the $Li^+$ first solvation shell was significantly reduced. The decrease of the EC self-diffusion coefficients is accounted for by noting that 4 out of 10 EC are diffusing with $Li^+$ having the lowest diffusion coefficient. A decreased overall solvent diffusion leads to increased viscosity that is responsible for slowing down $TFSI^-$ anions.

At the final stage of our analysis of the $Li^+$ transport mechanism, the temperature dependence of the EO/$Li^+$ residence is compared with the overall $Li^+$ diffusion coefficient as a function of temperature in Figure 9. Similar temperature dependence of these two processes indicates that the contribution of the structure diffusion (solvent exchange) to the overall $Li^+$ transport is present at all temperatures as the same extent. Figure 9 also shows that the temperature dependence of conductivity is weaker than that for the $Li^+$ diffusion coefficient and inverse $Li^+$/EC residence times. Increased ion correlation with increas-

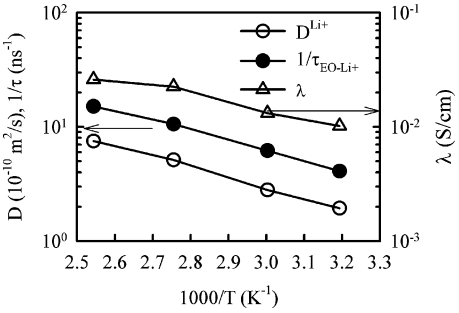


**Figure 9.** Temperature dependence of conductivity, $Li^+$ diffusion coefficient and inverse Li−Oc residence times ($1/\tau_{EO-Li^+}$) for EC:Li = 10.

ing temperature is the observed difference between temperature dependence of conductivity and ion self-diffusion.

## VI. Conclusions

MD simulations of EC/LiTFSI validated against available data for conductivity and self-diffusion coefficients were used to obtain fundamental understanding of ion clustering and cation transport mechanism. At the limit of completely dissociation, $Li^+$ was coordinated by 3.8 EC molecules. Increasing salt concentration resulted in replacing one EC molecule with one $TFSI^-$ anion contributing only one of its four oxygen atoms to the $Li^+$ first solvation shell. Formation of ion aggregates was observed. The probability of an ion to be a part on an aggregate of size *n* decreases exponentially with *n*. Ion aggregates contributed approximately 50% to the overall charge transport with another 50% contributed from free ion diffusion.

We have shown that the exchange of EC molecules between the first $Li^+$ coordination shell and outer shells accounts for half of the $Li^+$ diffusion leading to a picture that $Li^+$ transport occurs by a combination of the vehicular mechanism (diffusion with the solvation shell) and structure-diffusion resulting from exchange of molecules in the $Li^+$ first solvation shell and outer shells.

**Acknowledgment.** The authors are indebted to Subcontract LBL #6515401 for financial support.

**Supporting Information Available:** Text describing and a table giving force field parameters used in MD simulations of dissociated electrolyte and dissociated electrolyte with reduced EC exchange in the $Li^+$ first solvation shell. This material is available free of charge via the Internet at http://pubs.acs.org.

## References and Notes

(1) Hayamizu, K.; Aihara, Y.; Arai, S.; Martinez, C. G. *J. Phys. Chem. B* **1999**, *103*, 519−524.

(2) Soetens, J.-C.; Millot, C.; Maigret, B. *J. Phys. Chem. A.* **1998**, *102*, 1055.

(3) Li, T.; Balbuena, P. B. *J. Electrochem. Soc.* **1999**, *146*, 3613.

(4) Masia, M.; Probst, M.; Rey, R. *J. Phys. Chem. B.* **2004**, *108*, 2016.

(5) Newman, J.; Thomas, K. E.; Hafezi, H.; Wheller, D. R. *J. Power Sources* **2003**, *119*−*121*, 838−843.

(6) Masia, M.; Rey, R. *J. Phys. Chem. B.* **2004**, *108*, 17992.

(7) Borodin, O.; Smith, G. D. *J. Phys. Chem. B* Submitted for publication.

(8) Lucretius, www.che.utah.edu/∼gdsmith.

(9) Martyna, G. J.; Tuckerman, M.; Tobias, D. J.; Klein, M. L. *Mol. Phys.* **1996**, *87*, 1117.

(10) Ryckaert, J. P.; Ciccotti, G.; Berendsen, H. J. C. *J. Comput. Phys.* **1977**, *23*, 327.

(11) Martyna, G. J.; Tuckerman, M.; Tobias, D. J.; Klein, M. L. *Mol. Phys.* **1996**, *87*, 1117.

(12) Hyodo, S. A.; Okabayashi, K. *Electrochem. Acta* **1989**, *34*, 1551.

(13) Fukushima, T.; Matsuda, Y.; Hashimoto, H.; Arakawa, R. *Electrochem. Solid State Lett.* **2001**, *4* (8), A127−A128.

(14) Wang, Y. X.; Balbuena, P. B. *Int. J. Quantum Chem.* **2005**, *102*, 724−733.

(15) Wang, Y. X.; Balbuena, P. B. *J. Phys. Chem. A* **2002**, *106*, 9582−9594.

(16) Israelachvili, J. *Intermolecular & Surface Forces*; Academic Press: San Diego, CA, 1992.

(17) Dudley, J. T.; et al. *J. Power Sources* **1991**, *35*, 59.

(18) Tokuda, H.; Muto, S.; Hoshi, N.; Minakata, T.; Ikeda, M.; Yamamoto, F.; Watanabe, M. *Macromolecules* **2002**, *35*, 1403.